European Congress on Computational Methods
in Applied Sciences and Engineering (ECCOMAS 2012)
J. Eberhardsteiner et.al. (eds.)
Vienna, Austria, September 10-14, 2012

ON THE TIME-STEPPING STABILITY OF CONTINUOUS MASS-LUMPED AND DISCONTINUOUS GALERKIN FINITE ELEMENTS FOR THE 3D ACOUSTIC WAVE EQUATION

Elena Zhebel[1], **Sara Minisini**[1], **and Wim A. Mulder**[1,2]

[1]Shell Global Solutions International
PO Box 60, 2280 AB Rijswijk, The Netherlands,
Elena.Zhebel@shell.com

[2] Delft University of Technology, Faculty of Civil Engineering and Geosciences
PO Box 5048, 2600 GA Delft, The Netherlands

Keywords: stability, mass lumping, finite elements, discontinuous Galerkin, acoustic wave equation

Abstract. *We solve the three-dimensional acoustic wave equation, discretized on tetrahedral meshes. Two methods are considered: mass-lumped continuous finite elements and the symmetric interior-penalty discontinuous Galerkin method (SIP-DG). Combining the spatial discretization with the leap-frog time-stepping scheme, which is second-order accurate and conditionally stable, leads to a fully explicit scheme. We provide estimates of its stability limit for simple cases, namely, the reference element with Neumann boundary conditions, its distorted version of arbitrary shape, the unit cube that can be partitioned into 6 tetrahedra with periodic boundary conditions, and its distortions. The CFL stability limit contains a length scale for which we considered different options. The one based on the sum of the eigenvalues of the spatial operator for the first degree mass-lumped element gives the best results. It resembles the diameter of the inscribed sphere but is slightly easier to compute. The stability estimates show that mass-lumped continuous and SIP-DG finite elements have comparable stability conditions, with the exception of the elements of the first degree. The stability limit for the mass-lumped elements is less restrictive and allows for larger time steps.*

1 INTRODUCTION

Solving the three-dimensional wave equation remains a challenging problem in geophysical applications, especially for seismic imaging of the subsurface. Traditionally, the wave equation is solved with finite-difference methods. However, their accuracy deteriorates in complex geological settings with sharp contrasts in the medium and with topography. Finite elements on tetrahedral meshes are more flexible and accurate if the mesh follows the geometry of the interfaces and of the topography. We focus on two methods: the mass-lumped continuous finite elements [1, 2] and the symmetric interior-penalty discontinuous Galerkin (SIP-DG) method [3], since both allow for explicit time stepping. Because mass lumping of standard finite elements leads to a degradation of the accuracy, except for the standard linear element, polynomials of higher degree have to be added in the interior of the element. For 3D, tetrahedral elements of degree two [1] and three [2] are known. By borrowing nodes from higher-degree elements on the faces and in the interior, the mass matrix is made diagonal while preserving the accuracy of the spatial discretization. The SIP-DG method allows for the approximating functions to be discontinuous at the element interfaces. However, to impose continuity, additional terms called fluxes have to be included. The fluxes in an element consist of the outgoing fluxes and the contribution of the incoming fluxes across faces from the neighbouring elements. The discontinuous representation leads to a local mass matrix that can be easily inverted.

Combining the spatial discretization with the leap-frog time-integration scheme, which is second-order accurate and conditionally stable, leads to a fully explicit method. We have discussed the accuracy in an earlier paper [4]. Here, we will focus on the time-stepping stability for continuous mass-lumped and SIP-DG finite elements. Ideally, the stability condition is split into a mesh-independent constant CFL and mesh-dependent properties. It is generally of the form $\Delta t \leq \texttt{CFL} \min_\tau(d_\tau/c_\tau)$, where Δt is the time step, c_τ is local velocity in element τ, d_τ is the diameter of τ, to be specified, and CFL is a mesh-independent constant. In order to estimate the stability constant CFL [5] for mass-lumped and SIP-DG tetrahedral finite elements, we consider a number of simplified problems: the reference element with Neumann boundary conditions, its distorted version of arbitrary shape, the unit cube that can be partitioned into 6 tetrahedra with periodic boundary conditions, and its distortions. For SIP-DG, we also consider the unit cube and its distortions with zero values for the solution in neighbouring elements. The estimates for CFL are obtained by numerical optimization for these examples.

The paper is organized as follows. Section 2 describes the Fourier analysis for mass-lumped continuous and SIP-DG finite elements and suggests several choices for the diameter d. The stability estimates for continuous mass-lumped finite elements on different geometries are given in the Section 3. Section 4 lists CFL values for the SIP-DG method on the reference element as well as on the unit cube with 6 tetrahedra and periodic boundary conditions. Section 5 summarizes the conclusions.

2 METHOD

We consider the scalar wave equation for constant-density acoustics,

$$\frac{1}{c^2}\frac{\partial^2 u}{\partial t^2} - \Delta u = s, \tag{1}$$

on a bounded domain $\Omega \subset \mathbb{R}^3$ with velocity $c(\mathbf{x})$, pressure $u(\mathbf{x}, t)$ at time t and position $\mathbf{x} = (x, y, z) \in \Omega$ and source $s(\mathbf{x}, t)$. Here we discretize (1) with continuous mass-lumped and symmetric interior-penalty discontinuous Galerkin finite elements (SIP-DG).

The weak formulation for the continuous finite elements is given by

$$\int_\Omega c^{-2} v \frac{\partial^2 u}{\partial t^2}\, d\Omega - \int_\Omega \nabla u\, \nabla v\, d\Omega - \int_{\partial\Omega} (\mathbf{n}\cdot\nabla u) v d\Omega = \int_\Omega vs\, d\Omega,$$

$\forall v \in H^1(\Omega)$, $t \in (0,T)$, $u : (0,T)\times\mathbb{R}^3(\Omega) \to H^1(\Omega)$. After discretization with mass-lumped continuous finite elements, the spatial operator is given by

$$\mathcal{L} = \mathcal{M}^{-1}\mathcal{K}, \tag{2}$$

where $\mathcal{M}$ is the diagonal mass matrix and $\mathcal{K}$ is the stiffness matrix.

The weak formulation in case of discontinuous Galerkin finite elements is given by

$$\int_\Omega c^{-2} v \frac{\partial^2 u}{\partial t^2}\, d\Omega - \int_\Omega \nabla u\, \nabla v\, d\Omega - \int_{\Gamma} (\mathbf{n}\cdot\nabla u) v d\Omega = \int_\Omega vs\, d\Omega. \tag{3}$$

for all test functions v that are chosen as polynomials up to degree M. Here, $\mathbf{n}$ denotes the outward normal and Γ consists of internal and external boundaries of the domain Ω. For the discontinuous Galerkin finite elements, the solution is discontinuous across the internal boundaries. The term with the normal in 3, called flux term, is given by

$$-\int_\Gamma [u]\{\nabla v\}\, d\Omega + \epsilon \int_\Gamma [v]\{\nabla u\}\, d\Omega + \gamma \int_\Gamma [u][v]\, d\Omega.$$

If u^+ is the solution inside the element and u^- lives on one of the neighbouring elements, then $[u] := u^+ - u^-$ denotes the jump across the element boundary and $\{u\} := \frac{1}{2}(u^+ + u^-)$ is the average, whereas γ is a penalty parameter.

Expressing the solution in the basis of the test functions, $u(x,y,z,t) = \sum u_j(t) v_j(x,y,z)$, the flux term for a face F for each element is given by

$$\begin{aligned} &-\tfrac{1}{2}\textstyle\int_F (\nabla v_j\cdot\mathbf{n})^+ v_i^+ u_j^+ ds + \tfrac{\epsilon}{2}\int_F (\nabla v_i\cdot\mathbf{n})^+ v_j^+ u_j^+ ds + \gamma\int_F u_j^+ v_j^+ v_i^+ ds \\ &-\tfrac{1}{2}\textstyle\int_F (\nabla v_j\cdot\mathbf{n})^- v_i^+ u_j^- ds - \tfrac{\epsilon}{2}\int_F (\nabla v_i\cdot\mathbf{n})^+ v_j^- u_j^- ds - \gamma\int_F u_j^- v_j^- v_i^+ ds \end{aligned}$$

Note that SIP-DG has $\epsilon = -1$. Discretizing the weak formulation (3), we obtain the spatial operator for each element

$$\mathcal{L} = \mathcal{M}^{-1}\left(\mathcal{K} + \mathcal{F}^+ + \mathcal{F}^-\right), \tag{4}$$

where $\mathcal{M}$ and $\mathcal{K}$ are the local mass and stiffness matrix, respectively. We also have the contribution of the fluxes. The term $\mathcal{F}^+$ denotes the sum of the outgoing fluxes over the four faces in the given element. The second term $\mathcal{F}^-$ contains the incoming fluxes from the four neighbouring elements.

In the absence of a source term, the standard second-order discretization in time of (1) gives

$$\mathbf{u}^{n+1} - 2\mathbf{u}^n + \mathbf{u}^{n-1} = \Delta t^2 c^2 \mathcal{L}\mathbf{u}^n, \tag{5}$$

where $\mathcal{L}$ is a spatial discretization operator. We assume that the velocity c is constant within an element. Here, $\mathbf{u}^n$ characterizes the discrete solution at time $t_n = t_0 + n\Delta t$, $n = 0, 1, \ldots$. In the scalar case, we can perform a Fourier transform in time. Let G be the growth factor of the solution after a time step. Its corresponding Fourier symbol is $\hat{G} = e^{i\omega\Delta t}$. Then, equation (5) reduces to

$$\hat{G} - 2 + \hat{G}^{-1} = 4\nu,$$

with $\nu = \frac{1}{4}\Delta t^2 c^2 \mathcal{L}$. The roots of the above equation are

$$\hat{G} = 1 - 2\nu \pm 2\imath\sqrt{\nu(1-\nu)}$$

and obey $|\hat{G}| \leq 1$ if $0 \leq \nu \leq 1$. Otherwise, at least one of the solutions has $|\hat{G}| > 1$ and the time-stepping scheme is unstable. Stability leads to the requirement

$$\Delta t \leq \frac{2}{c\sqrt{\rho(\mathcal{L})}}. \tag{6}$$

Since the spectral radius in (6) contains information about the mesh, the question is how to express this stability condition into a a mesh-independent constant `CFL` and mesh-dependent properties. A simple scaling argument suggests an expression of the form

$$\Delta t \leq \min_{\tau} \sigma_\tau \frac{d_\tau}{c_\tau}, \tag{7}$$

of the ratio of some diameter d_τ and the velocity c_τ per element and the minimum is taken over all elements τ. Ideally, the number σ_τ should be independent of τ and be equal to a constant number `CFL`. This Courant-Friedrichs-Lewy number [5] can be taken as $\texttt{CFL} = 2/(d\sqrt{\rho(\mathcal{L})})$, using the spectral radius ρ of the spatial operator $\mathcal{L}$ and the largest diameter d over all elements.

For higher-order time stepping, `CFL` has to be multiplied by a constant factor, for instance, by $\sqrt{3} = 1.73$ for fourth-order time stepping [6].

We have not been able to find a measure d in (7) that produces a value of σ that is independent of the problem, but some choices are better than others. As an example, consider the single reference element with vertices $(0,0,0)$, $(1,0,0)$, $(0,1,0)$, and $(0,0,1)$. If this is discretized with a degree 1 mass-lumped finite element with homogeneous Neumann boundary conditions, the stiffness matrix $\mathcal{K}$ and lumped mass matrix $\mathcal{M}$ are

$$\mathcal{K} = \frac{1}{6}\begin{pmatrix} 3 & -1 & -1 & -1 \\ -1 & 1 & 0 & 0 \\ -1 & 0 & 1 & 0 \\ -1 & 0 & 0 & 1 \end{pmatrix}, \quad \mathcal{M} = \frac{1}{24}\begin{pmatrix} 1 & & & \\ & 1 & & \\ & & 1 & \\ & & & 1 \end{pmatrix}.$$

Following [7], we can consider a version of this element on an arbitrary tetrahedron and compute the eigenvalues of $\mathcal{L} = \mathcal{M}^{-1}\mathcal{K}$. One of those is zero and the other three are the roots of

$$\lambda^3 - \beta\lambda^2 + \gamma\lambda - \delta = 0, \tag{8}$$

with

$$\beta = 4J_0^{-2}\sum_{k=1}^{4} A_k^2, \quad \gamma = 16J_0^{-2}\sum \ell_j^2, \quad \delta = 256J_0^{-2},$$

where A_k is the area of face k, ℓ_j the length of edge j, and $J_0 = 6V$ with V the volume of the tetrahedron. Note that $\beta = \sum_{j=1}^{3}\lambda_j$ is the sum and $\delta = \prod_{j=1}^{3}\lambda_j$ the product of the non-zero eigenvalues. By symmetry of the spatial operator, all eigenvalues are non-negative, so $0 \leq \lambda_j \leq \beta$. We will consider the following 4 choices for a diameter d:

- $d_i = 2J_0/\sum_{k=1}^{4} A_k$, the diameter of the inscribed sphere,
- $d_l = \min_j \ell_j$, the length of the shortest edge,

- $d_b = 2/\sqrt{\beta}$, based on the sum of the eigenvalues mentioned above, or
- $d_e = 2/\sqrt{\max_j \lambda_j}$.

To see which of these choices produces a nearly constant σ, we first consider the same case as before, but let the reference element have a varying height. Then, the four vertices are $(0,0,0)$, $(1,0,0)$, $(0,1,0)$, and $(0,0,h)$. In this case, $J_0 = h$ and

$$\begin{aligned} d_i &= 2h/(1+2h+\sqrt{1+2h^2}), \\ d_l &= \min(1,h), \\ d_b &= h/\sqrt{2+4h^2}, \\ d_e &= h/\sqrt{2(2+3h^2+\sqrt{4-h^2(4-9h^2)})}. \end{aligned}$$

The coefficients in (8) are $\beta = 16 + 8/h^2$, $\gamma = 48 + 96/h^2$, and $\delta = 256/h^2$, leading to eigenvalues 4 and $2h^{-2}(2+3h^2 \pm \sqrt{4-4h^2+9h^4})$, apart from the zero eigenvalue. For stability, we can define

$$\texttt{CFL} = \min_h \sigma(h), \quad \sigma(h) = \frac{2}{d(h)\sqrt{\lambda_{\max}}}, \quad \lambda_{\max} = \frac{2}{h^2}\left(2+3h^2+\sqrt{4-4h^2+9h^4}\right),$$

where $d(h)$ can be one of the four choices mentioned above. By definition, $\sigma(h) = 1$ for $d(h) = d_e$. Figure 1 displays $\sigma(h)$ for the other three choices of $d(h)$. Clearly, d_b is the second best in the sense that it has the smallest variation with h, namely $\sqrt{3/2}$ or about 22%.

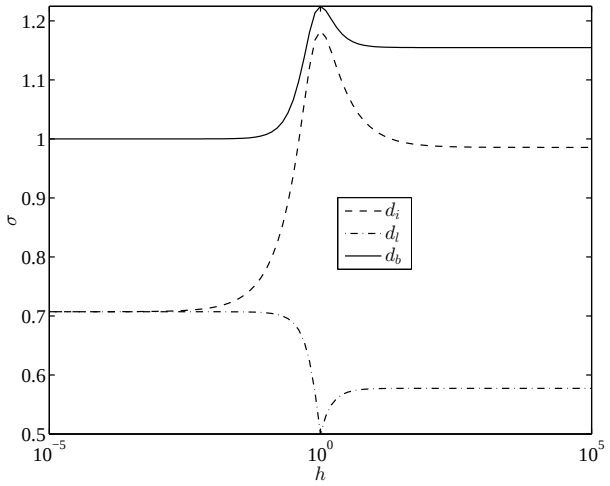

Figure 1: Graph of $\sigma(h)$ for three choices of $d(h)$.

The idea of the stability analysis described in this paper is to estimate the spectral radius of the spatial discretization operator, in our case the mass-lumped continuous finite element operator and SIP-DG operator. One way to obtain estimates is by considering a single reference element and distorted version of it. These can be obtained by the coordinate transform

$$\begin{pmatrix} x_1' \\ x_2' \\ x_3' \end{pmatrix} = \begin{pmatrix} 1 & p_1 & q_1 \\ 0 & p_2 & q_2 \\ 0 & 0 & q_3 \end{pmatrix} \begin{pmatrix} x_1 \\ x_2 \\ x_3 \end{pmatrix}, \tag{9}$$

where $p_2 > 0$ and $q_3 > 0$. Other shapes follow by symmetry. To avoid too strong distortions, we require $d_o/d_i \leq 100$, where d_o is the diameter of the circumscribed and d_i or the inscribed sphere. Even poor mesh generation software will be able to construct tetrahedra with this property.

Fourier or plane-wave analysis of the spatial operator is a natural approach in a finite-difference setting with a regular Cartesian grid. The method is also applicable to finite elements if the regular Cartesian grid is used packed with tetrahedra. Here, we select a cube divided into 6 tetrahedra as shown on Figure 2. Note that this cube also contains the reference element with a diameter of the inscribed sphere $0.423 = 1 - 1/\sqrt{3}$. The diameters of the inscribed sphere for the 6 tetrahedra in the cube are either 0.360 or 0.423. As with the single tetrahedron, we can consider distorted versions by using the coordinate transform (9).

The following cases will be considered:

1. Reference element with homogeneous Neumann boundary conditions (mass-lumped) or zero values in neighbouring elements (DG);

2. distorted versions of the reference element;

3. unit cube containing 6 tetrahedra with periodic boundary conditions;

4. distorted versions of the latter.

For the Fourier case, we will estimate the smallest and largest occurring value of

$$\sigma(p_1, p_2, q_1, q_2, q_3) = \frac{2}{\sqrt{\lambda_{\max}}} \frac{1}{\max_\tau d}, \quad \lambda_{\max} = \max_{\xi_1,\xi_2,\xi_3} \rho(\bar{\mathcal{L}})$$

using $d = d_i$, d_b, d_e, and d_l, respectively. Here, the ξ_k are normalized wavenumbers, specified below, and $\bar{\mathcal{L}} = \mathcal{M}^{-1}\mathcal{K}$ is the spatial operator with periodic boundary conditions. Note that d and $\bar{\mathcal{L}}$ depend on the five parameters p_1, p_2, q_1, q_2, and q_3. For the single reference element and its distorted version, $\lambda_{\max} = \rho(\bar{\mathcal{L}})$, the largest eigenvalue of the operator. We used the Nelder-Mead method [8] for finding the extremum. Since this method is not guaranteed to converge to the global minimum or maximum, several runs with random starting values were performed. In this way, we increased the chance of reaching the global extremum.

The shortest edge length, d_l, resulted in extremely large variations of the estimates, so will not be considered further on.

Next, we will review the continuous mass-lumped and the SIP-DG elements separately and provide stability estimates for each.

3 MASS-LUMPED CONTINUOUS FINITE ELEMENTS

We consider the four geometries described above. The construction of the matrices is straightforward for the reference element and its distorted versions. Imposing periodic boundary conditions for the 6 tetrahedra requires additional calculations.

To build the matrix $\bar{\mathcal{L}} = \mathcal{M}^{-1}\mathcal{K}$ with periodic boundary conditions, we assembled the matrices $\mathcal{M}$ and $\mathcal{K}$ for a configuration of $3^3 = 27$ unit cubes on the domain $[-1, 2]^3$. Let $\mathcal{N}$ denote set of degrees of freedom in the central unit cube $[0, 1)^3$. We arrange the numerical solution of (1) on the nodes $\mathcal{N}$ in a vector. The subset of the matrix $\bar{\mathcal{L}}$ that has rows corresponding to the nodes inside $[0, 1)^3$ acts on this vector as well as on the degrees of freedom in neighbouring cubes.

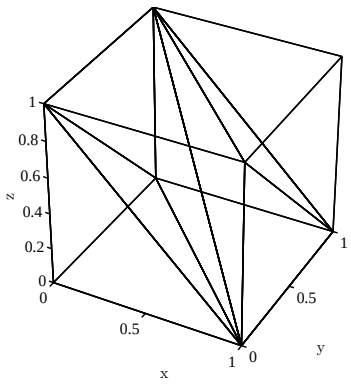

Figure 2: Unit cube packed with 6 tetrahedral elements, one of them is the reference element.

We introduce shift operators T_j, $j = 1, 2, 3$ in the x_j-direction with the property that

$$T_j^s u(x_1, x_2, x_3) = u(x_1 + s\delta_{1j}, x_2 + s\delta_{2j}, x_3 + s\delta_{3j}),$$

where $\delta_{ij} = 1$ if $i = j$ and 0 otherwise. The Fourier symbol of T_j is

$$\hat{T}_j = \exp(\imath k_j \Delta x_j),$$

where Δx_j is the grid spacing in coordinate direction j, in this case of unit length, and k_j is the wavenumber in each coordinate direction. Let us denote $\xi_j = k_j \Delta x_j$ with $\xi \in (-\pi, \pi]$, then

$$\hat{T}_j = \exp(\imath \xi_j).$$

The shift operators enable straight-forward expression of the values of the degrees of freedom in the neighbouring to $[0, 1)^3$ cubes.

With this plane wave decomposition, the Fourier symbol of $\bar{\mathcal{L}}$ is readily obtained. Its components are

$$\hat{\mathcal{L}}_{l,m} = \sum_n \bar{\mathcal{L}}_{l,n} [\hat{T}_1^{s_1}]_{n,m} [\hat{T}_2^{s_2}]_{n,m} [\hat{T}_3^{s_3}]_{n,m},$$

with integer shifts s_j, $j = 1, 2, 3$, in each coordinate. The sum over n involves those indices for which $\bar{\mathcal{L}}_{l,n}$ is not zero and for which the coordinate shifts are zero ($n = m$) or $\pm\Delta x_j$ (neighbouring elements), where $\Delta x_j = 1$. Generalization to distorted elements is almost trivial.

Table 1: Values of `CFL` based on the spectral radius for a single reference element with homogeneous Neumann boundary conditions for various mass-lumped elements of degree M. The first three columns are based on the reference element, using d_i, d_b or d_e, but these values are too optimistic. The second set is based on optimization over eigenvalue computations for single tetrahedral elements of arbitrary shape. The values in brackets correspond to the largest value of σ for the elements considered.

M	type	d_i	d_b	d_e	d_i		d_b		d_e	
1		1.18	1.22	1	0.72	(1.73)	1	(1.73)	1	(1)
2		0.090	0.093	0.076	0.062	(0.118)	0.079	(0.118)	0.068	(0.099)
3	1	0.059	0.061	0.050	0.042	(0.062)	0.056	(0.062)	0.036	(0.062)
3	2	0.105	0.109	0.089	0.072	(0.121)	0.096	(0.121)	0.070	(0.112)

Table 1 lists the values of `CFL` for the mass-lumped reference element as well as the smallest and largest (in brackets) values obtained for a single distorted element for three choices of the

Table 2: Values of CFL based on the spectral radius for an unit cube with periodic boundary conditions for various mass-lumped elements of degree M. The left part of the table shows CFL values for an unit cube with periodic boundary conditions. The values in the right part of the table are based on optimization over eigenvalue computations for unit cube of arbitrary shape with periodic boundary conditions. Values without brackets and values in brackets correspond to the smallest and the largest value of σ, respectively.

M	type	d_i	d_b	d_e	d_i		d_b		d_e	
1		1.30	1.34	1.01	0.85	(1.41)	1.01	(1.41)	0.77	(1.41)
2		0.104	0.107	0.081	0.070	(0.117)	0.094	(0.117)	0.063	(0.111)
3	1	0.056	0.058	0.044	0.036	(0.062)	0.048	(0.062)	0.034	(0.060)
3	2	0.104	0.107	0.082	0.066	(0.120)	0.088	(0.120)	0.065	(0.105)

diameter. The first set of 3 columns refers to the reference element. The last set of 6 columns is obtained by optimizing over the distorted reference element, with the largest minimum in brackets. Note that the estimates for the reference element are somewhat optimistic. For d_e, we observe no variation for the continuous mass-lumped element of degree 1, by definition. For higher-order elements however, the smallest variation appears to be obtained for d_b. Note that the continuous mass-lumped element of degree 3 has a more favourable stability limit for type 2 than for type 1 [2]. The reader should bear in mind that, since these results were obtained by numerical optimization, there is chance that the global extrema were missed.

Table 2 shows the smallest and the largest (in brackets) CFL values for unit cube packed with 6 tetrahedra with periodic boundary conditions as well as its distorted versions for three choices of the diameter. Again, d_b provides the smallest ratio over different distortions.

4 DISCONTINUOUS GALERKIN FINITE ELEMENTS

To estimate the spectral radius of the SIP-DG spatial operator, we performed stability analysis on the reference element and its distorted versions as well as the unit cube with 6 tetrahedra and periodic boundary conditions as shown on Figure 3 and its distortions. As in case of mass-lumped continuous elements, the two last cases need additional computations for each set of wavenumbers.

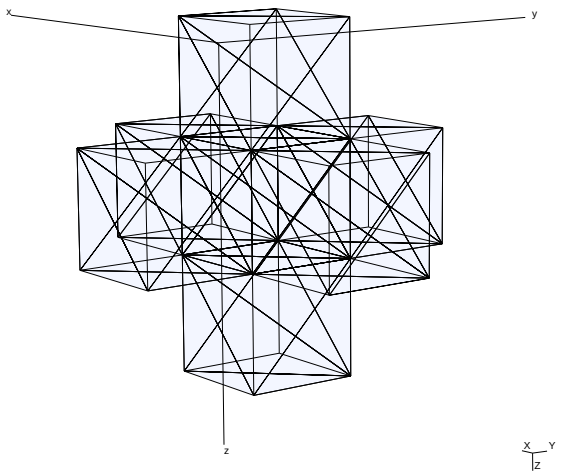

Figure 3: Unit cube with its neighbours for DG.

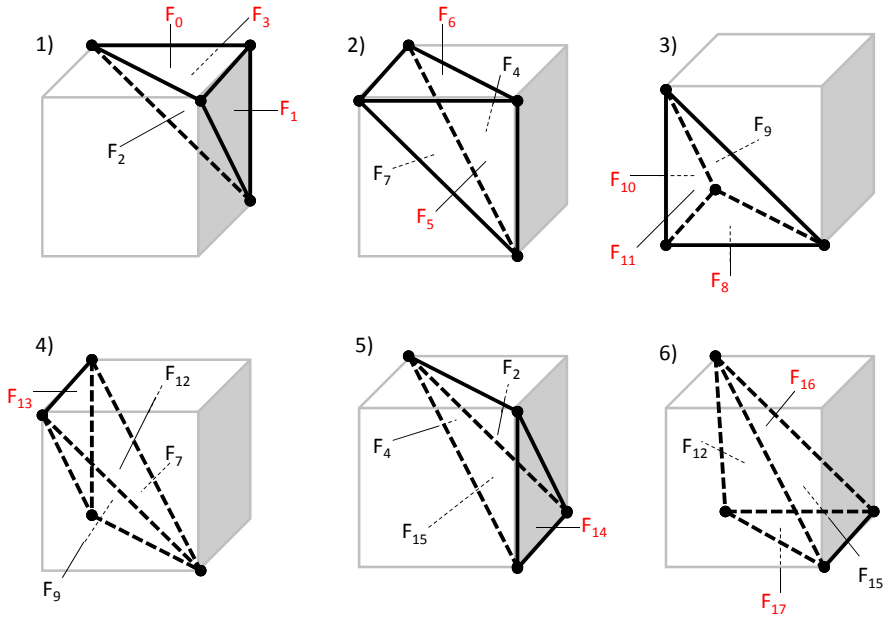

Figure 4: Unit cube with 6 tetrahedra. The internal and external faces are marked with black and red color, respectively.

Considering the unit cube with 6 tetrahedra and natural boundary conditions, the stiffness matrix of the spatial operator including fluxes is given by

$$\begin{pmatrix} \mathcal{K}+\mathcal{F}^+ & & & & \mathcal{F}_2^- & \\ & \mathcal{K}+\mathcal{F}^+ & & \mathcal{F}_7^- & \mathcal{F}_4^- & \\ & & \mathcal{K}+\mathcal{F}^+ & \mathcal{F}_9^- & & \\ & \mathcal{F}_7^- & \mathcal{F}_9^- & \mathcal{K}+\mathcal{F}^+ & & \mathcal{F}_{12}^- \\ \mathcal{F}_2^- & \mathcal{F}_4^- & & & \mathcal{K}+\mathcal{F}^+ & \mathcal{F}_{15}^- \\ & & & \mathcal{F}_{12}^- & \mathcal{F}_{15}^- & \mathcal{K}+\mathcal{F}^+ \end{pmatrix}$$

where each line of the matrix represents an element and the subscript of the fluxes from neighbouring tetrahedra identifies the number of the face, see Figure 4. The mass matrix is a block diagonal matrix consisting of local mass matrices.

In order to add periodic boundary conditions, let us introduce shift operators similar to the mass-lumped continuous elements. The components of the periodic spatial operator are then given by $\hat{T}_j^s \mathcal{F}_m^-$, where $\mathcal{F}_m^-$, denotes a face adjacent to neighbouring elements outside the unit cube. The Fourier symbol of the periodic spatial operator is then computed as

$$\hat{\mathcal{L}} = \mathcal{M}^{-1} \begin{pmatrix} \mathcal{K}+\mathcal{F}^+ & \hat{T}_2\mathcal{F}_3^- & & \hat{T}_1\mathcal{F}_1^- & \mathcal{F}_2^- & \hat{T}_3\mathcal{F}_0^- \\ \hat{T}_2^{-1}\mathcal{F}_5^- & \mathcal{K}+\mathcal{F}^+ & \hat{T}_3\mathcal{F}_6^- & \mathcal{F}_7^- & \mathcal{F}_4^- & \\ & \hat{T}_3^{-1}\mathcal{F}_8^- & \mathcal{K}+\mathcal{F}^+ & \mathcal{F}_9^- & \hat{T}_1^{-1}\mathcal{F}_{10}^- & \hat{T}_2^{-1}\mathcal{F}_{11}^- \\ \hat{T}_1^{-1}\mathcal{F}_{13}^- & \mathcal{F}_7^- & \mathcal{F}_9^- & \mathcal{K}+\mathcal{F}^+ & & \mathcal{F}_{12}^- \\ \mathcal{F}_2^- & \mathcal{F}_4^- & \hat{T}_1\mathcal{F}_{14}^- & & \mathcal{K}+\mathcal{F}^+ & \mathcal{F}_{15}^- \\ \hat{T}_3^{-1}\mathcal{F}_{17}^- & & \hat{T}_2\mathcal{F}_{16}^- & \mathcal{F}_{12}^- & \mathcal{F}_{15}^- & \mathcal{K}+\mathcal{F}^+ \end{pmatrix}.$$

The spectral radius ρ is the largest eigenvalue of the Fourier symbol of the spatial operator, $\hat{\mathcal{L}}$, over all sets of scaled wavenumbers $\{\xi_1, \xi_2, \xi_3\}$ and can again be found by a numerical maximization algorithm.

For the penalty parameter, we generalize the approach proposed by [9] to three dimensions with $\gamma = (M+1)(M+2)(M+3)/(12\mathcal{A})$, where M is the degree of the finite element and $\mathcal{A}$ is the area of a face in the given mesh.

Table 1 lists the values of CFL for the SIP-DG reference element as well as the smallest and largest (in brackets) values obtained for a single distorted element for three choices of the diameter. The first set of 3 columns refers to the reference element. The last set of 6 columns is obtained by optimizing over the distorted reference element, with the largest minimum in brackets.

The results based on the unit cube packed with 6 tetrahedra with periodic boundary conditions as well as its distorted versions are given in Table 2. The smallest and the largest (in brackets) CFL values are shown for for three choices of the diameter. Again, d_b provides the smallest ratio over different distortions.

Table 3: Values of CFL based on the spectral radius for a single reference element with homogeneous Neumann boundary conditions for various single SIP-DG element of degree M. The first three columns are based on the reference element, using d_i, d_b or d_e, but these values are too optimistic. The second set is based on optimization over eigenvalue computations for single tetrahedral elements of arbitrary shape. The values in brackets correspond to the largest value of σ for the elements considered. The first four rows were obtained for an element with homogeneous Neumann boundary conditions implying zero fluxes. The last four rows were obtained for a DG element with interior fluxes only, so with a zero solution in the neighbours.

M	type	d_i	d_b	d_e	d_i		d_b		d_e	
1	DG	0.53	0.55	0.45	0.32	(0.77)	0.45	(0.77)	0.45	(0.45)
2		0.27	0.28	0.23	0.18	(0.37)	0.23	(0.37)	0.22	(0.25)
3		0.17	0.175	0.143	0.119	(0.23)	0.14	(0.23)	0.13	(0.16)
4		0.118	0.122	0.100	0.083	(0.16)	0.100	(0.16)	0.094	(0.116)
1	DG+F	0.33	0.34	0.28	0.18	(0.35)	0.21	(0.45)	0.17	(0.45)
2		0.19	0.19	0.16	0.098	(0.20)	0.113	(0.24)	0.095	(0.24)
3		0.12	0.12	0.102	0.062	(0.13)	0.071	(0.15)	0.054	(0.15)
4		0.083	0.086	0.070	0.042	(0.086)	0.049	(0.101)	0.043	(0.101)

Table 4: Values of CFL based on the spectral radius for a unit cube packed with 6 tetrahedral SIP-DG elements of degree M with periodic boundary conditions (left part of the table) and its distortions (right part of the table). The values in the right part of the table are based on optimization over eigenvalue computations for arbitrarily distorted unit cubes, but with the constraint that $d_o/d_i \leq 100$. Values without brackets and values in brackets correspond to the smallest and the largest value of σ, respectively.

M	d_i	d_b	d_e	d_i		d_b		d_e	
1	0.24	0.25	0.19	0.16	(0.27)	0.22	(0.36)	0.146	(0.36)
2	0.133	0.138	0.104	0.088	(0.15)	0.120	(0.20)	0.081	(0.20)
3	0.086	0.089	0.067	0.056	(0.097)	0.077	(0.121)	0.053	(0.123)
4	0.059	0.061	0.046	0.039	(0.067)	0.053	(0.085)	0.036	(0.083)

5 CONCLUSIONS

Estimates of the stability constant were considered for the continuous mass-lumped and symmetric interior-penalty DG (SIP-DG) finite elements. Different choices of the measure of element size were suggested such as the diameter of the inscribed sphere, the length of the shortest edge and measures based on the spectral properties of the spatial operator for the lowest-degree mass-lumped finite element on a single tetrahedron with natural boundary conditions. Based

on each measure, the values of the CFL-number, CFL, were computed for both methods on the reference element as well as a single tetrahedral element of arbitrary shape. Also, the unit cube packed with 6 tetrahedra and periodic boundary conditions was considered. We found that the smallest variation of CFL appears to be obtained for the measure based on the sum of the eigenvalues for the above-mentioned lowest-degree mass-lumped element, both for the higher-order continuous mass-lumped elements as well as for the SIP-DG elements. This measure resembles the expression for the diameter of the inscribed sphere but has a slightly lower computational cost.

The first-degree mass-lumped elements have a much larger CFL, allowing for a larger time step than required for SIP-DG. The CFL for elements of second degree are comparable for both schemes. Of the two variants of the third degree mass-lumped element, the second allows for a larger time step than the cubic SIP-DG. Since mass-lumped elements of degree 4 and higher are presently unknown, only stability results for SIP-DG were given. The general trend for SIP-DG is that CFL becomes smaller for higher-order elements. Performance and accuracy comparisons for these methods were considered elsewhere [4].

References

[1] W. A. Mulder. A comparison between higher-order finite elements and finite differences for solving the wave equation. In J.-A. Désidéri, P. LeTallec, E. Oñate, J. Périaux, and E. Stein, editors, *Proceedings of the Second ECCOMAS Conference on Numerical Methods in Engineering*, pages 344–350. John Wiley & Sons, Chichester, 1996.

[2] M. J. S. Chin-Joe-Kong, W. A. Mulder, and M. van Veldhuizen. Higher-order triangular and tetrahedral finite elements with mass lumping for solving the wave equation. *Journal of Engineering Mathematics*, 35(4):405–426, 1999.

[3] M. F. Weeler. An elliptic collocation-finite element method with interior penalties. *SIAM Journal on Numerical Analysis*, 15(1):152–161, 1978.

[4] S. Minisini, E. Zhebel, A. Kononov, and W. A. Mulder. Efficiency comparisons for higher-order continuous mass-lumped and discontinuous Galerkin finite-element methods for the 3-D acoustic wave equation. 74th EAGE Conference & Exhibition, Extended Abstracts, A004, Copenhagen, Denmark, June 2012.

[5] R. Courant, K. Friedrichs, and H. Lewy. Über die partiellen Differenzengleichungen der mathematischen Physik. *Mathematische Annalen*, 100(1):32–74, 1928.

[6] M. A. Dablain. The application of high-order differencing to the scalar wave equation. *Geophysics*, 51(1):54–66, 1986.

[7] J. R. Shewchuk. What is a good linear finite element? – interpolation, conditioning, anisotropy, and quality measures. Technical report, In Proc. of the 11th International Meshing Roundtable, 2002.

[8] J. A. Nelder and R. Mead. A simplex method for function minimization. *Computer Journal*, 7(4):308–313, 1965.

[9] M. Ainsworth, P. Monk, and W. Muniz. Dispersive and dissipitive properties of discontinuous Galerkin finite element methods for the second-order wave equation. *Journal of Scientific Computing*, 27(1-3):5–40, 2006.